Analytical Chemistry: A Journal (2023)
Clausius Scientific Press, Canada

DOI: 10.23977/analc.2023.020104
ISSN 2616-1958 Vol. 2 Num. 1

# *Density Functional Theory Investigation on Five-coordinated Iron Porphyrin Compounds*

**Yikun Zhou[1,2], Xianqiang Chen[1,3], Jie Zheng[1], Jing Huang[1,3,*]**

*[1]Fujian Provincial Key Laboratory of Ecology-Toxicological Effects and Control for Emerging Contaminants, College of Environmental and Biological Engineering, Putian University, Putian, Fujian, 351100, China*
*[2]College of Chemical Engineering, Huaqiao University, Xiamen, Fujian, 361021, China*
*[3]Key Laboratory of Ecological Environment and Information Atlas, Fujian Provincial University, Putian, Fujian, 351100, China*
*[*]Corresponding author*

***Keywords:*** Penta-coordinated iron porphyrins, Fluorinated porphyrins, Electronic structure

***Abstract:*** This manuscript focuses on the quantum chemistry of five-coordinated iron porphyrin compounds [Fe ($T^{i}PrP$) X] (X=F,Cl,I). Iron porphyrins are the core structures of heme enzymes, such as cytochrome P450 monooxygenase, peroxidase or catalase, whose active centers are iron porphyrin structures. The synthetic metalloporphyrin model has been widely applied to the study of mechanisms and intermediates of heme enzyme-related biological reactions, and metalloporphyrin catalysis provides new synthetic methods for important chemicals. In this paper, the geometric configuration of selected molecules was optimized using Gaussian 09 software. The geometric configuration optimization process was calculated using the heterogeneous density generalized theory B3LYP. To better investigate the electronic structure and orbital distribution of [Fe($T^{i}PrP$) X] (X=F,Cl,I), based on the molecular structure of the previous step, the Sddall basis group and Sddall pseudopotential were used for the Fe atoms and the all-electron 6-311G++(d,p) basis group was used for the rest of the atoms.

## 1. Introduction

Iron (III) haloporphyrin plays a key role in the biological olfaction of heme enzyme, and provides a greener way for the oxidation of organic compounds. For example, fluorinated porphyrin, as a component of photonic materials, has multifunctional photophysics, electron absorption property and antioxidant degradation. [1-7]. IThe use of metalloporphyrin models has brought important insights into the mechanism and intermediates of biological reactions [8-11]. Bionic models are advantageous because they are easier to obtain and handle than biocatalysis systems, and halogenated metalloporphyrin is one of the earliest, most effective and powerful catalytic systems. [12, 13]

[Fe($TE^{t}PrP$) X] where X = $F^-$, $Cl^-$, $Br^-$, $I^-$ and $ClO_4^-$ compounds that have been experimentally, while the F, C1 and Br complexes adopt high spin S=5/2 states, the I complexes exhibit a mixed intermediate spin state in $CD_2C1_2$ solution. Depending on the strength of the axial ligand field, iron (III) porphyrin complexes containing anionic axial ligands typically show high spin (S=5/2) or mixed

intermediate spin (S=3/2, 5/2) states. Halides as axial ligands always exhibit a high spin (S=5/2) state, while halides containing perchlorate exhibit a mixed intermediate spin (S=3/2, 5/2) state. However, if porphyrins are replaced by porphyrin analogues such as porphyrins, the situation is completely different; Not only perchlorate but also iodine complexes show a fairly pure intermediate spin state. These results are attributed to short Fe-NP bond lengths, narrow cavity regions surrounded by four nitrogen atoms, and small deviations of iron atoms from the mean porphyrin plane. Even in porphyrin complexes, conditions for a stable intermediate spin state can be met if the porphyrin ring is deformed.

In this study, we used the density functional theory [14] to investigate the structure of the electrons of the five-coordinated iron porphyrin compounds from the perspective of theoretical chemistry. The studied system is shown in Figure 1, where the iron atom is coordinated to the four nitrogen atoms of the porphyrin ring and also to the halogens (F, Cl, I) to form a five-coordinated iron structure with isopropyl substitution on the four sides of the iron porphyrin [15].

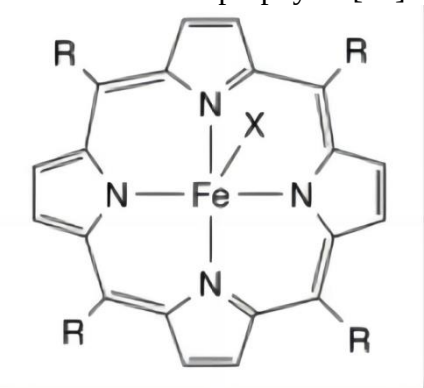


(R=$^{i}$Pr, X= F, Cl, I)

Figure 1: The five-coordinated iron porphyrin system studied in this study

## 2.1. Conformation Optimization

Gaussian 09 software was used to optimize the geometric configuration of selected molecules. The geometric configuration optimization process was calculated using the heterogeneous density functional theory B3LYP. Past studies have shown that the B3LYP generalized function is more reliable for geometry optimization and quantum calculations of electronic structures of iron porphyrins. [16-21] For fluoro- and chlorine-substituted five-coordinated iron porphyrins, the Lanl2DZ basis group and the Lanl2DZ pseudo-potential[18] are used for the Fe atoms, and the all-electron 6-31G(d,p) basis group is used for the rest of the atoms. For iodine-substituted five-coordinated iron porphyrins, the Lanl2DZ group and Lanl2DZ pseudopotential are used for the Fe and iodine atoms, and the all-electron 6-31G (d,p) group is used for the rest of the atoms. In this study, the structure of the five-coordinated iron porphyrins in a nonpolar $CH_2Cl_2$ solvent was considered, so the solventization model was used in the optimization process. In this study, IEFPCM in Gaussian program was used as the solvent model, customizing the nonpolar $CH_2Cl_2$ solvent dielectric constant of 9.08. After optimization, we used Gaussview program to read the molecular geometrical configuration and molecular orbitals.

## 2.2. Energy and Orbital Analysis

To better investigate the electronic structure and orbital distribution of [Fe ($T^{i}$ PrP)X] (X=F,Cl,I), based on the molecular structure in the previous step, the Sddall group and Sddall pseudopotential were used for the Fe atom, and the all-electron 6-311G++ (d,p) group was used for the rest of the atoms. For iodine-substituted five-coordinated iron porphyrins, the Sddall group and Sddall

pseudopotential were used for the Fe and iodine atoms, and the all-electron 6-311G++ (d,p) group was used for the rest of the atoms. The solventization was performed using IEFPCM as the solvent model, customizing the nonpolar $CH_2Cl_2$ solvent dielectric constant of 9.08 and the temperature defined as 298 K. In addition, natural orbital NBO calculations were performed in this study to obtain the electronic arrangement of Fe atoms at various multiple weights.

## 3. Results and Discussion

### 3.1. Geometric Structure Optimization

#### 3.1.1. Optimized geometry of [Fe ($T^iPrP$) F] molecules

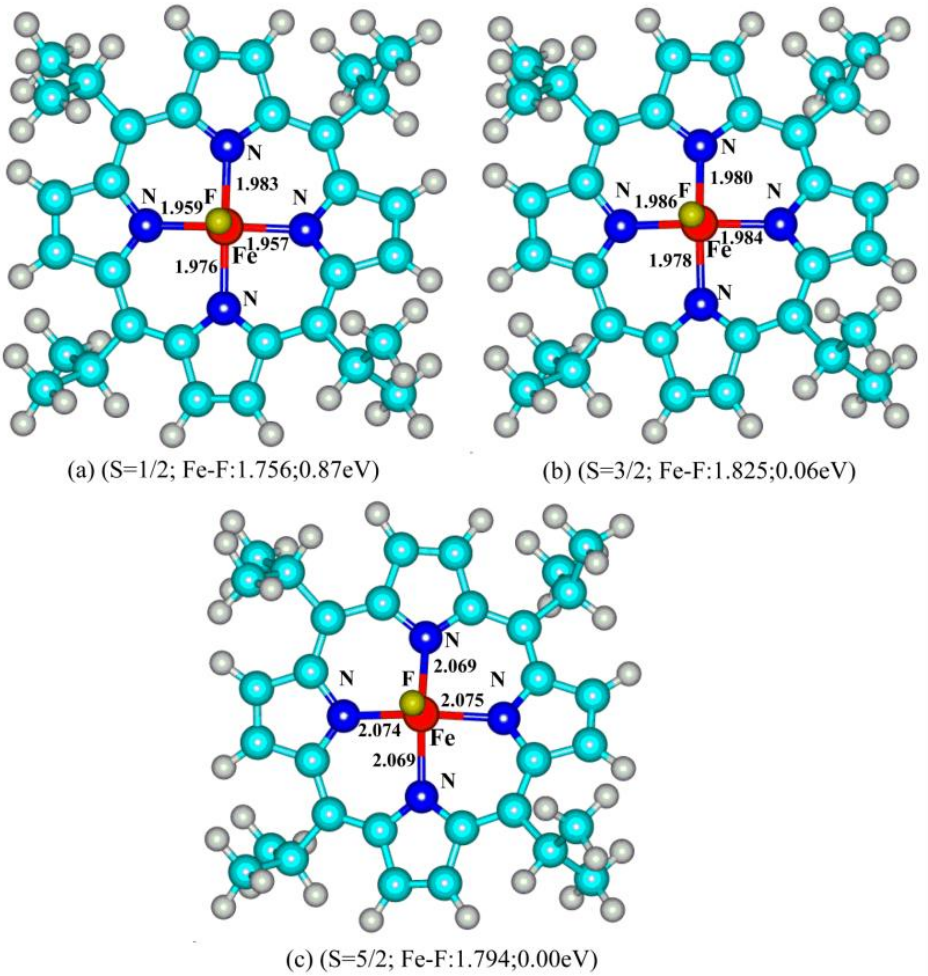


Figure 2: Optimized geometry of [Fe ($T^iPrP$) F] molecule

The optimized geometries of the [Fe ($T^iPrP$) F] molecules in the duplex, quadruplet and hexadruplet states are shown in Figure 2. The length of Fe-N bond increases gradually with the increase of the multiplet degree. For example, the Fe-N bond of the doppelganger state (S = 1/2) is about 1.95-1.98 Å, the Fe-N bond of the quadruplet state (S = 3/2) is about 1.97-1.99 Å, and the Fe-N bond of the sextuplet state (S = 5/2) is about 2.06-2.08 Å. In terms of system energy, the [Fe($T^iPrP$)F] molecule of the sextuplet state (S=5/2) has the lowest energy, and the quadruplet state (S =3/2) system energy is 0.06 eV higher than that of the sextuple state (S=5/2), and the duple state (S=1/2) system energy is 0.87 eV higher than that of the sextuple state (S=5/2), so the most stable of the nonpolar

$CH_2Cl_2$ solvents is the sextuple state (S=5/2) at 298 K. This conclusion is consistent with the results of the NMR measurements from literature experiments.

### 3.1.2. Optimized geometry of [Fe (TiPrP) Cl] molecules

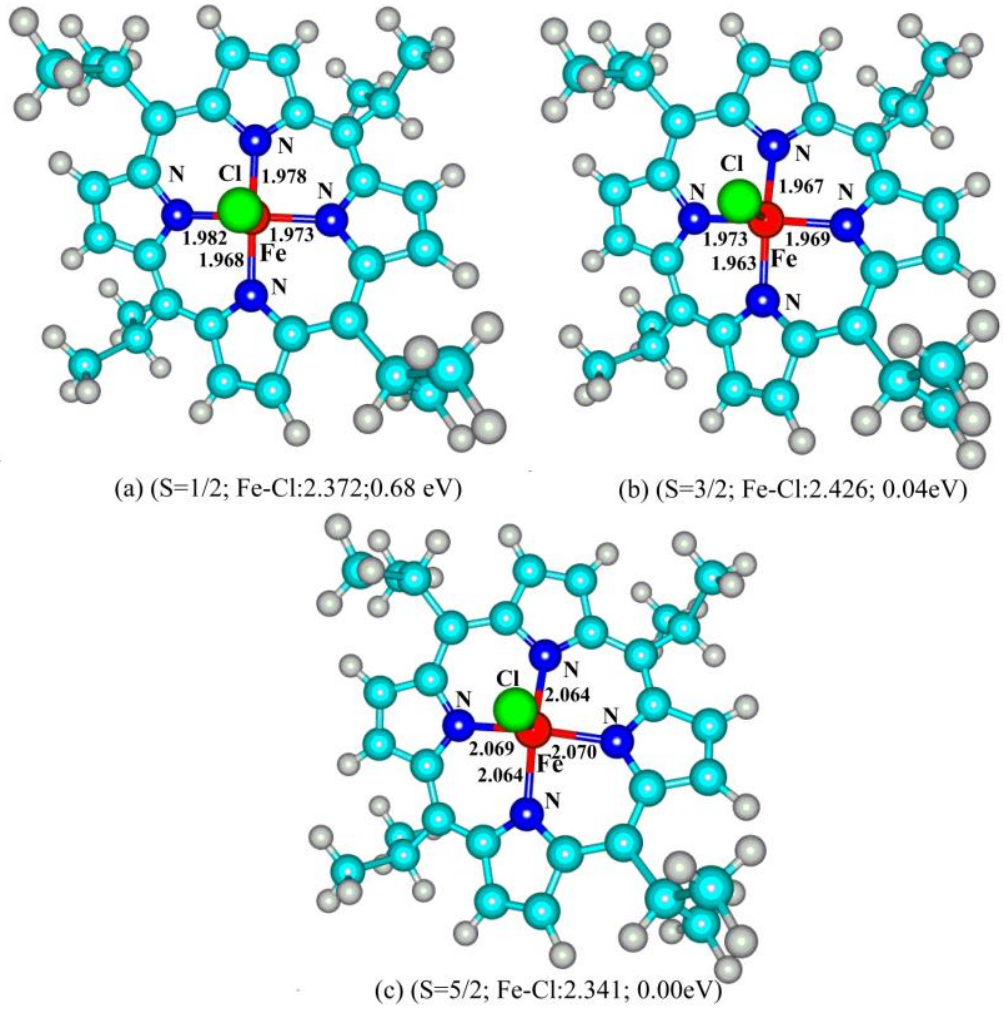


Figure 3: Optimized geometry of [Fe ($T^iPrP$) Cl] molecule

The optimized geometries of [Fe ($T^iPrP$)Cl] molecules in the duplex, quadruplex and hexa states are shown in Figure 3. Similar to [Fe ($T^iPrP$)F], for the [Fe($T^iPrP$)Cl] system, the lowest energy electronic state is also the six-fold state (S=5/2), which is in agreement with the experimental NMR measurements. In the six-fold state [Fe ($T^iPrP$)Cl] system, the Fe-N coordination bond length of Fe-N with the porphyrin ring is 2.06-2.07 Å, and the Fe-Cl bond length is 2.341 Å.

### 3.1.3. Optimized geometry of [Fe ($T^iPrP$) I] molecules

The optimized geometries of [Fe ($T^iPrP$) I] molecules in the duplex, quadruplex and hexa states are shown in Figure 4. The Cartesian coordinates of the structures of the various electronic states are shown in Appendix 1. Unlike [Fe ($T^iPrP$)F] and [Fe($T^iPrP$)Cl], the most stable electronic state for the [Fe($T^iPrP$)I] system is also the quadruplet state (S=3/2), which is consistent with the conclusions obtained from experimental NMR measurements. In the quadruplet state [Fe($T^iPrP$)I] system, the Fe-N coordination bond length of Fe-N with the porphyrin ring is 1.94-1.96 Å and the Fe-I bond length is 3.059 Å.

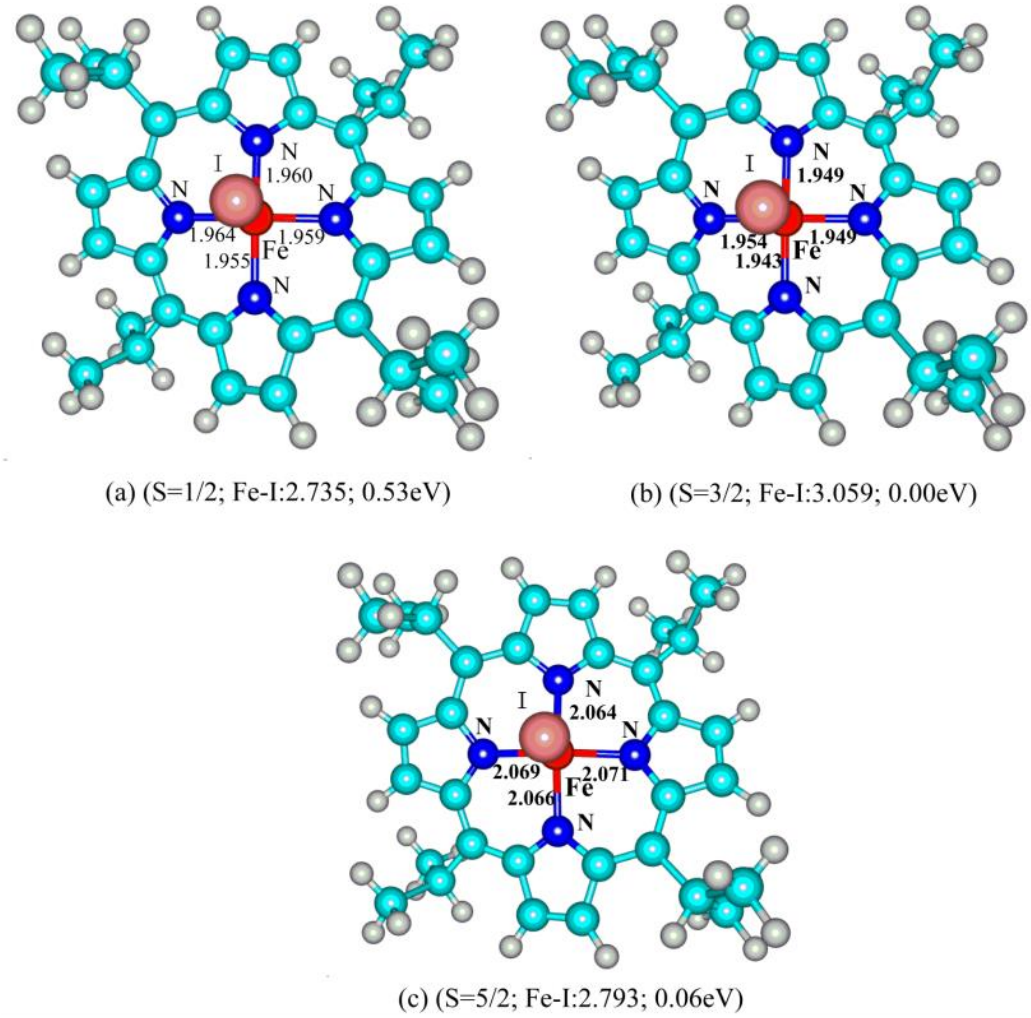


Figure 4: Optimized geometry of [Fe ($T^i$PrP)I] molecule

## 3.2. Electronic Structure Analysis

### 3.2.1. [Fe ($T^i$ PrP) F] and [Fe($T^i$ PrP)Cl] Natural Orbital Analysis

From the energy analysis of the previous system, it is known that the most stable electronic states of [Fe($T^i$ PrP)F] and [Fe($T^i$ PrP)Cl] are sixfold (S=5/2), i.e.The whole molecular system has five single electrons, and it is known from the orbital analysis that these five single electrons are mainly arranged in the five d-rails from Fe to the porphyrin ring, and the electrons are arranged in the Fe valence electrons as $(d_{xy})^1$ $(d_{yz})^1$ $(d_{xz})^1$ $(d_{x2-y2})^1$ $(d_{z2})^1$. The five d orbitals of the Fe atom are not simple due to the fact that the coordination case of Fe is pentacoordinated, not a uniform potential field and the difference in d orbital symmetry. For the [Fe ($T^i$PrP) F] system, the $d_{xy}$ orbital energy is the lowest, and the $d_{yz}$ and $d_{xz}$ energies are comparable, being 2.83 kcal/mol and 2.90 kcal/mol higher than $d_{xy}$ , respectively. The $d_{x2-y2}$ orbital energy is 3.19 kcal/mol higher than the lowest $d_{xy}$, and the $d_{z2}$ orbital energy is the highest, being 12.65 kcal/mol higher than $d_{xy}$. The [Fe($T^i$PrP)Cl] system The orbital arrangement and valence electron distribution of [Fe($T^i$PrP)F] system are similar to those of [Fe($T^i$PrP)F] system. The valence electron orbitals and valence electron arrangement of F-substituted and Cl-substituted Fe are shown in Figure 5, and their arrangement and orbital energy order are consistent with the experimentally determined structures.

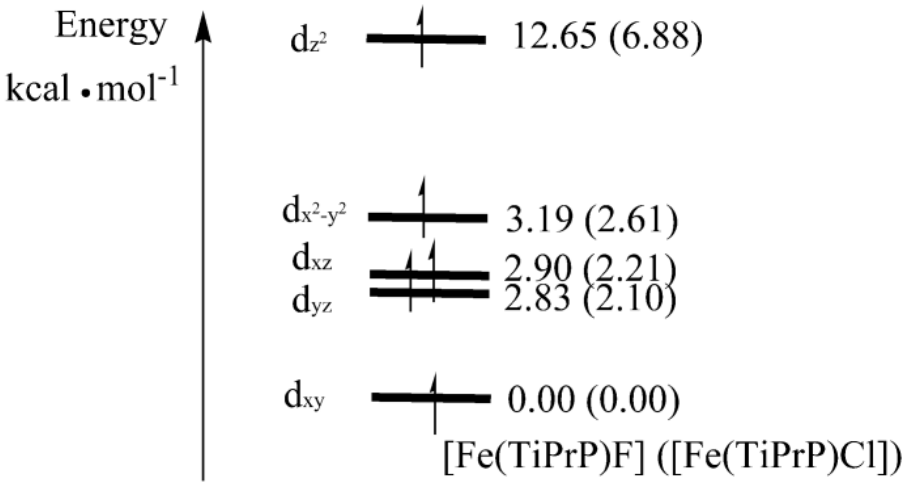


Figure 5: Energy distribution of d orbitals and valence electron arrangement of Fe atoms in [Fe ($T^iPrP$)F] and [Fe($T^iPrP$)Cl] systems

### 3.2.2. Natural Orbital Analysis of [Fe ($T^iPrP$) I

From the energy analysis of [Fe($T^iPrP$)I] system, it is known that the most stable electronic state of [Fe($T^iPrP$)I] is the quadruplet state (S=3/2), i.e. The whole molecular system has three single electrons. From the results of natural orbital analysis, it is known that the Fe valence electron arrangement has six electrons and the electronic grouping is $(d_{xy})^2(d_{yz})^1(d_{xz})^1(d_{x2-y2})^1(d_{z2})^1$. The five d orbitals of Fe atoms are not simple because of the coordination case of Fe is five-coordinated, not uniform potential field and the difference of d orbital symmetry. Fe-I bond bond length is 3.059Å and Fe-I bonding is weak.The electronic grouping of Fe is closer to the four-coordinated case, and the energy difference of d orbital energy level of each Fe is large, as in Figure 6. For the [Fe($T^iPrP$)I] system, the $d_{xy}$ orbital energy For the [$T^iPrP$)I] system, the $d_{z2x2-y2}$ orbital energy is higher than the lowest $d_{xy}$ by 18.17kcal/mol, the d orbital energy is higher than the lowest $d_{xy}$ by 18.65kcal/mol, and the $d_{yz}$ and $d_{xz}$ energies are higher than dxy by 20.26kcal/mol and 20.28kcal/mol, respectively.

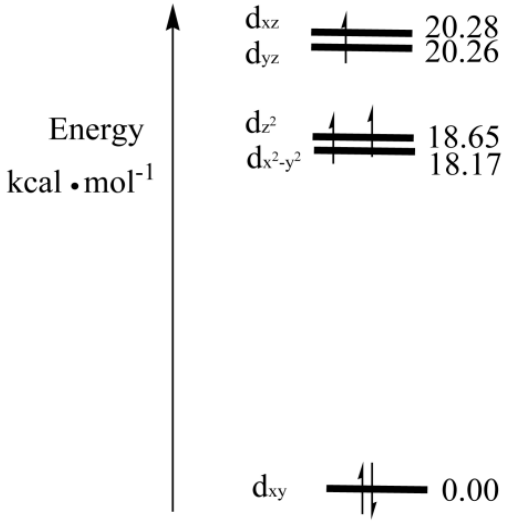


Figure 6: D-orbital energy distribution and valence electron arrangement of Fe atoms in the [Fe ($T^iPrP$)I] system

## 4. Conclusion

The length of Fe-N bond increases gradually with the increase of the multiplet degree. For example, the Fe-N bond of the doppelganger state (S=1/2) is about 1.95-1.98 Å, the Fe-N bond of the tetraplex state (S=3/2) is about 1.97-1.99 Å, and the Fe-N bond of the sextuplex state (S=5/2) is about 2.06-2.08 Å. In terms of system energy, the [Fe($T^iPrP$)F] molecule of the sextuplex state (S=5/2) has the lowest energy, the tetraplex state ( S=3/2) system energy is higher than that of the sextuple state (S=5/2), and the duple state (S=1/2) system energy is higher than that of the sextuple state (S=5/2), so the most stable of the nonpolar $CH_2Cl_2$ solvents is the sextuple state (S=5/2) at 298 K. This conclusion is consistent with the results of the NMR measurements of the literature experiments.

Similar to [Fe ($T^iPrP$)F], for the [Fe($T^iPrP$)Cl] system, the lowest energy electronic state is also the six-fold state (S=5/2), which is in agreement with the experimental NMR measurements. Unlike [Fe($T^i$ PrP)F] and [Fe($T^i$ PrP)Cl], for the [Fe($T^iPrP$)I] system, the most stable electronic state is also the quadruplet state (S=3/2), which is consistent with the experimental NMR measurements.

The most stable electronic states of [Fe ($T^iPrP$)F] and [Fe($T^iPrP$)Cl] are sixfold (S=5/2), i.e. and the whole molecular system has five single electrons, which are mainly arranged in the five d orbitals from Fe to the porphyrin ring as shown by the orbital analysis, and the electrons in the Fe valence electron arrangement are $(d_{xy})^1(d_{yz})^1(d_{xz})^1(d_{x2-y2})^1$ $(d_{z2})^1$. The five d orbitals of the Fe atom are not concise due to the fact that the coordination situation of Fe is five-coordinated, not a uniform potential field and the difference in d-orbital symmetry.


## Acknowledgements

We thanks the Fujian Provincial Natural fund (No.2020J05210, No.2021J011105, No. 2022J01132911. No. 2022J01132905); Fujian Provincial Department of Education Teaching and Research Project (JAT220303); Fujian Provincia Science and Technology Commissioner (202135030079).


## References


*[1] Bhupathiraju, N. V. S. D. K., Rizvi, W., Batteas, J. D., and Drain, C. M. (2016). Fluorinated porphyrinoids as efficient platforms for new photonic materials, sensors, and therapeutics. Organic and biomolecular chemistry, 14 (2), 389–408.*

*[2] Ko, Y. J., Yun, K. J., Kang, M. S., Park, J., Lee, K. T., Park, S. B., and Shin, J. H. (2007). Synthesis and in vitro photodynamic activities of water-soluble fluorinated tetrapyridylporphyrins as tumor photosensitizers. Bioorganic and medicinal chemistry letters, 17 (10), 2789–2794.*

*[3] Milot, R. L., and Schmuttenmaer, C. A. (2015). Electron injection dynamics in high-potential porphyrin photoanodes. Accounts of chemical research, 48 (5), 1423–1431.*

*[4] Nakazono, T., Parent, A. R., and Sakai, K. (2015). Improving singlet oxygen resistance during photochemical water oxidation by cobalt porphyrin catalysts. Chemistry, 21 (18), 6723–6726.*

*[5] Aggarwal, A., Bhupathiraju, N. V. S. D. K., Farley, C., and Singh, S. (2021). Applications of Fluorous Porphyrinoids: An Update. Photochemistry and photobiology, 97 (6), 1241–1265.*

*[6] Liu, W., and Groves, J. T. (2015). Manganese Catalyzed C-H Halogenation. Accounts of chemical research, 48 (6), 1727–1735.*

*[7] Balding, P. R., Porro, C. S., McLean, K. J., Sutcliffe, M. J., Mar échal, J. D., Munro, A. W., and de Visser, S. P. (2008). How do azoles inhibit cytochrome P450 enzymes? A density functional study. The journal of physical chemistry. A, 112 (50), 12911–12918.*

*[8] Cocco, G., Cocco, A., Sollai, F., Sanjust, E., and Zucca, P. (2017). Bioinspired versus Enzymatic Oxidation of Some Homologous Thionine Dyes in the Presence of Immobilized Metalloporphyrin Catalysts and Ligninolytic Enzymes. International journal of molecular sciences, 18 (12), 2553.*

*[9] Kubota, R., Asayama, S., and Kawakami, H. (2014). A bioinspired polymer-bound Mn-porphyrin as an artificial active center of catalase. Chemical communications (Cambridge, England), 50 (100), 15909–15912.*

*[10] Mahammed A. and Gross Z. (2011). The importance of developing metal complexes with pronounced catalase-like activity. Catalysis Science and Technology, 1, 535–540.*

*[11] Rajakumara, E., Saniya, D., Bajaj, P., Rajeshwari, R., Giri, J., and Davari, M. D. (2022). Hijacking Chemical Reactions of P450 Enzymes for Altered Chemical Reactions and Asymmetric Synthesis. International journal of molecular sciences, 24 (1), 214.*
*[12] Short, M. A., Sommer, R. D., Falzone, A. J., Huang, T., Weare, W. W., and Roizen, J. L. (2019). A five-coordinate iron (III) porphyrin complex including a neutral axial pyridine N-oxide ligand. Acta crystallographica. Section C, Structural chemistry, 75 (Pt 6), 717–722.*
*[13] Haedicke, I. E., Li, T., Zhu, Y. L. K., Martinez, F., Hamilton, A. M., Murrell, D. H., Nofiele, J. T., Cheng, H. M., Scholl, T. J., Foster, P. J., and Zhang, X. A. (2016). An enzyme-activatable and cell-permeable MnIII-porphyrin as a highly efficient T1 MRI contrast agent for cell labeling. Chemical science, 7(7), 4308–4317.*
*[14] Liu, Q. and Zhou, Z. (2009). Synthesis of iron porphyrins and their axial coordination properties. Journal of Hunan University of Science and Technology, 24 (03), 108-112.*
*[15] Zhang, X.Y., Cui, X., Wang, Y., Li, X., Zhang, G.Y. and Zhang, C. (2021). Synthesis of ferrocene porphyrin compounds and their substituent effects. Journal of Jilin University, 59 (02), 408-414.*
*[16] Huang, J. Yang, L. and Fu M. (2022). Theoretical investigations on the excited-state intramolecular proton transfer in the solvated 2-hydroxy-1-naphthaldehyde carbohydrazone. Open Chemistry, 20, 785-792.*
*[17] Huang, J., Li, F. and Qi Y. (2020). Comparative study on the impact of ethane/ethylene/acetylene addition on ignition of fuel-rich n-decane/air flame. UPB Scientific Bulletin, Series B, 82 (4), 185-198.*
*[18] Huang, J., Yang, L., Fu M., Chen Z., Liu W., Lin Y. and Yan Y. (2022). The effect of adding water electrolysis products on stability of the fuel-lean combustion in n-decane/air flames: a numerical study. UPB Scientific Bulletin, Series B, 84 (3), 109-120.*
*[19] Huang J., Ying, F., Su P. and Wu W. (2014). VBEFP/PCM: a QM/MM/PCM approach for valence-bond method and its application for the vertical excitations of formaldehyde and acetone in aqueous solution. Science China Chemistry, 57, 1409-1417.*
*[20] Ning, T., Song, J., Wew, J., Zhang. M., Lu, Q., Huang, J. and Li, C. (2018). Control of the electronic structure of manganese nitrido complexes by para ring substituents: a theoretical study. Chinese Journal of Structural Chemistry, 37, 1541-1549.*
*[21] Huang, J., Li, C., Wang, B., Sharon, D.A., Wu W. and Shaik, S. (2016). Selective chlorination of substrates by the halogenase SyrB2 is controlled by the protein according to a combined quantum mechanics/molecular mechanics and molecular dynamics study. ACS Catalysis 6, 2694−2704.*